Determining Heat Island Response to Varying Land Cover Changes Between 2004 and 2017 Within the City of Reno, Nevada

Brendan W. Lawrence
University of Nevada, Reno
Kenneth E. Nussear
University of Nevada, Reno
Jill S. Heaton
University of Nevada, Reno

Abstract

The objective of this research was to investigate the role of land cover changes through time in influencing spatial variability of the surface urban heat island of the metropolitan area of Reno-Sparks, Nevada. Thermal imagery from Landsat 7 ETM+ sensor was gathered for a period between 2004 and 2017. Using parcel data, the time series of Landsat data was sampled for areas that had undergone development during that time. A set of generalized linear models was conducted to determine expected temperature change with land cover class. It was found that recently developed regions within Reno-Sparks are 0.6°C warmer on average than the undeveloped desert grasses and sage. When wetlands/irrigated greenery were converted, it resulted in an increase of over 2°C. This research has shown that the Reno-Sparks surface urban heat island has undergone local, but measurable, growth in the past fourteen years.

Introduction

The Urban Heat Island (UHI) phenomenon describes a situation in which urban cores and developed areas exhibit higher surface and air temperatures than surrounding non-developed regions. This gradient in temperatures is caused by several factors; first and foremost it is induced by the transition of latent heat flux into sensible heat via the transformation of vegetative and soil surfaces to the lower albedo materials that are commonly found amongst city centers (Imhoff et al. 2010). Secondly, human-made materials such as asphalt and concrete absorb high amounts of solar radiation and release a percentage of it later in the day as sensible heat (Bokaie et al. 2016). Finally,

the introduction of high-rises and skyscrapers can inhibit prevailing wind patterns and prevent more even temperature gradients (Bokaie et al. 2016).

The intensity and impact of the UHI are of significant interest as the world's population is rapidly urbanizing, with as many as fifty-four percent of the global population residing in cities as of 2014, with estimates of around two-thirds of the world's population dwelling in cities by 2050 (United Nations 2014). An extensive proportion of the human population will be subjected to artificially increased temperatures that may be as high as or higher than 8°C above the surrounding regions (Imhoff et al. 2010). High spatial resolution data from the Airborne Thermal and Land Applications Sensor (ATLAS) shows surface temperature in microclimate extremes within a city to be as high as 60°C (Wang and Quattrochi 2007). The negative effects of such conditions include increased air pollution (Estoque et al. 2017), increased power consumption that may strain power grids (Azevedo et al. 2016), and increased severity of summertime heat waves, which claim thousands of lives in an average year (Mirzaei and Haghighat 2010). More rarely, prolonged or severe heat waves in populated regions can push death tolls into the tens of thousands (Robine et al. 2007). All of these consequences will be aggravated by larger-scale climate changes and continued migration into city centers (Jones et al. 2015).

Research shows the exact magnitude of UHI impacts to be more complex than a simple relationship to population growth as originally postulated by Oke (1973). While the general positive correlation of temperatures and population holds (Oke 1973), the temperature does not retain a set value above the surrounding areas. The temperature gradient is more pronounced depending on season and time of day (Wang and Quattrochi 2007). Atmospheric stability also plays a role in the day-to-day magnitude of the UHI phenomenon (Wang and Quattrochi 2007).

Space-borne remote-sensing systems are capable of analyzing UHI effects with a wide range of spatial and temporal scales when funding for a dedicated sensor and/or aerial missions is unavailable. These systems provide more complete coverage than station-based measurements. Data from many systems such as Landsat are free, and their thermal bands are proving to be of great use for studying UHI signals (Imhoff et al. 2010; Bokaie et al. 2016; Estoque et al. 2017). There are drawbacks, including but not limited to systematic errors in gain (Aniello et al. 1994) and distortions due to atmospheric conditions, both of which can be accounted for with pre-processing (Bokaie et al. 2016). Urban Heat Island and Surface Urban Heat Island signals may

be influenced by building height variability that exists within cities due to changes in shading throughout the day (Small and Zappa 2017). Deep street canyons show the same surface temperature as densely vegetated areas such as city parks during the afternoon hours (Small and Zappa 2017).

UHI research centered on larger cities (e.g., Phoenix and Las Vegas) utilized remote sensing techniques; lacking are similar studies on small to mid-sized cities. (Cayan and Douglas 1984; Xian and Crane 2006; Ramaurthy and Sangobanwo 2016). A case in point is the Reno-Sparks metropolitan area with its estimated population of more than 400,000 (Washoe County Consensus Forecast 2016). From the 1960s onward, a growing discrepancy exists between the minimum temperature records at the Reno/Tahoe International Airport and Tahoe, California (Ardnt and Redmond 2004). Comparisons with other rural stations show further contrast in temperatures and continuing UHI-driven warming in the intensely developed regions of Reno-Sparks (Hatchett et al. 2016).

Washoe County has undergone a large population expansion in the past several decades (Forstall 1996) that includes conversion of agricultural and wetlands in the south and east parts of the valley to developed lands. This may lead to an even hotter Reno-Sparks, as healthy vegetation plays an important role in mitigating the effects of the UHI (Akbari et al. 2001; Rahman et al. 2017). The Reno-Sparks area, the largest developed area within Washoe County, is categorized as mid-latitude steppe on the Köppen Climate Classification System, with a wide-swinging temperature range between seasons (Houghton et al. 1975). Precipitation is variable every year, as the Reno-Sparks Metropolitan area lies in the Sierra Nevadas' rain shadow. However, resting on the immediate leeward side of the rain shadow with an average elevation of 1,338 meters for the valley floor (U.S. Geological Survey 2006), the region still receives higher amounts of rainfall/snowfall than do lower basins to the east (Hatchett et al. 2016). Although the cities reside in a dry environment, the Truckee River flows through the area, creating an oasis for vegetation. Plants appropriate incoming shortwave solar insolation for food use and prevent the transformation into sensible heat (Rahman et al. 2017). Water uptake by vegetation also plays a role as a conduit for transpiration, which is a considerable heat sink (Gillner et al. 2015).

Current projections show the Reno-Sparks area gaining 100,000 additional inhabitants by the year 2036 (Washoe County Consensus Forecast 2016), and many Planned Unit Developments (PUDs) to house these individuals are slated for prime green space (Northern Nevada Regional Growth Study

2015); the summertime temperatures in the valley may start to negatively impact sensitive species in the urban environment (Mason et al. 2017).

This project analyzes alterations of land surface temperature in the urban environment of Reno-Sparks, using freely available imagery collected by the Landsat 7 Satellite's ETM+ (Enhanced Thematic Mapper Plus) sensor's thermal band. These data are the effective skin temperature or land surface temperature of all surfaces in the Landsat scene, which may be comprised of asphalt, vegetation, or building roof. This study did not make use of atmospheric corrections, as only relative temperature differences are being compared; absolute surface temperature was not required (Small and Zappa 2017).

In particular, this research addresses whether or not recent development of the region's desert landscape has made any quantifiable impact on the local surface urban heat island. Secondarily, the effect that irrigated and natural green space has, and how it acts, upon the local UHI signal is examined. Being able to detect fine-scale nuances in UHI impacts using freely available data should also allow a wider variety of growing urban areas to do simple assessments and create zoning plans for better future outcomes where artificial microclimate alterations are minimized.

Methods

The area of interest (Figure 1), is approximately 68,500 acres, filling the majority of the Truckee Meadows Valley and including the urban centers of both Reno and Sparks as well as the bulk of their developed townships. It also contains important features such as the Reno-Tahoe International Airport, as well as multiple large sections of crop land and natural wetlands.

Landsat 7's thermal band (Band 6) covers the window from 10.4 to 12.5 micrometers and has a native spatial resolution of sixty meters (U.S. Geological Survey -A 2018). The U.S. Geological Survey, however, resamples this band to thirty meters within its standard level-1 product to match the spatial resolution of the other sensors' bands using the Landsat Product Generation System (U.S. Geological Survey - B 2018). With this spatial resolution, distinct city morphologies can easily be detected and major landmarks such as dense city cores and airport runways are apparent (Figure 2). An issue with resolving individual buildings is that there are some examples of structures appearing to read between 10°C and -35°C within the city boundaries. This variation is most likely due to the emissivity of the building's metal roofs (Morton 2018). Some metals, especially highly reflective ones, have low emissivity

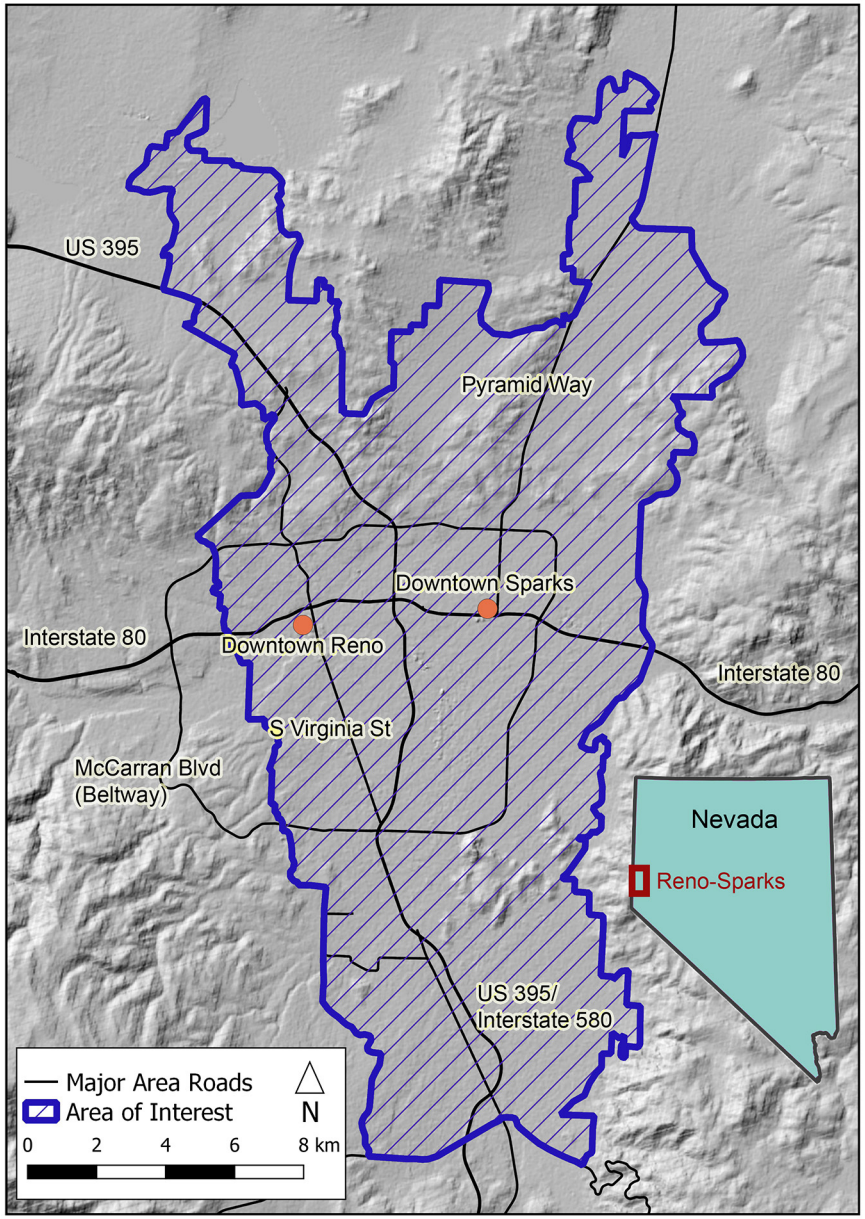

Figure 1.—Map of Reno-Sparks Urban AOI.

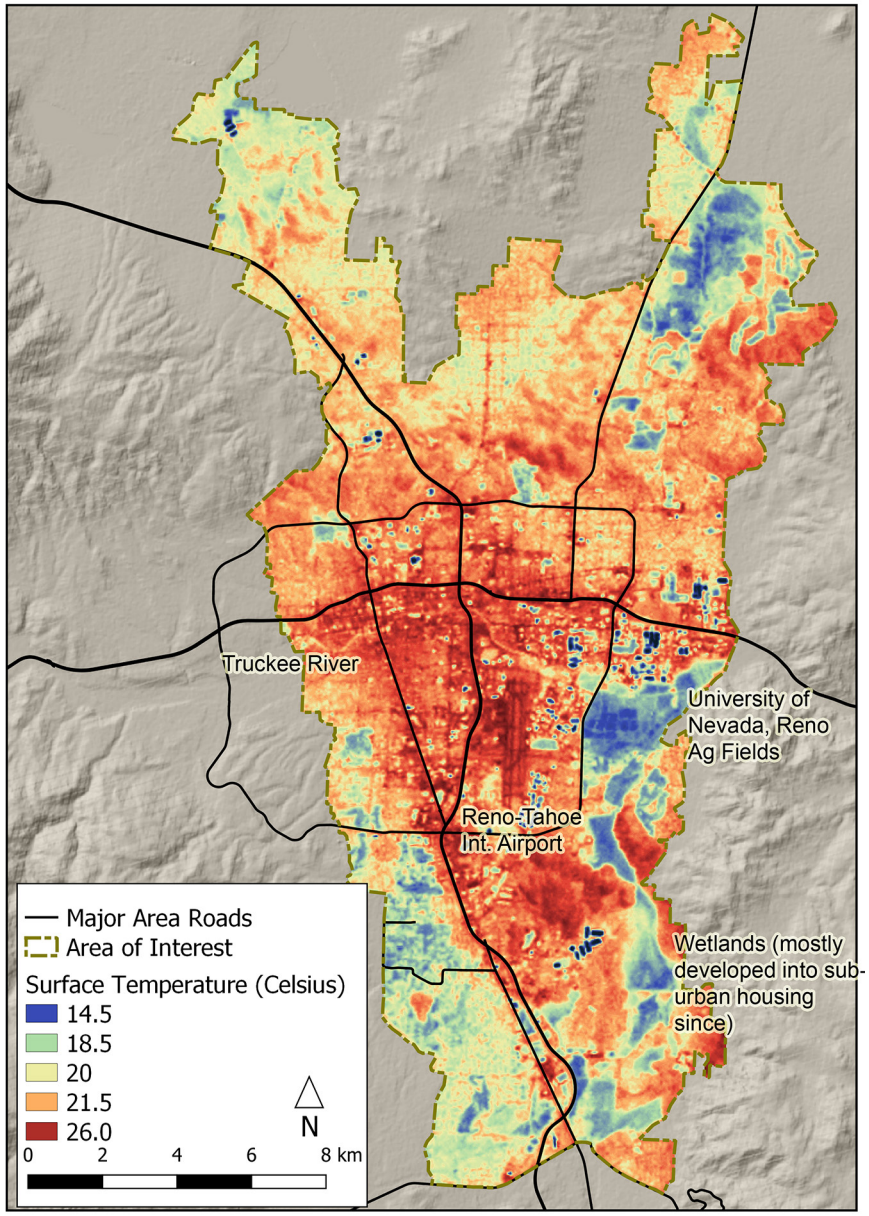

Figure 2.—Example of at-satellite surface temperature map: July 17, 2005). A direct comparison between an automated surface observing station located at Reno-Tahoe International Airport (toward the center of the area of interest polygon) and the underlying pixel show approximate temperatures of 27.8°C (air temperature for closest measurement to Landsat 7 flyover) and 24.0°C, respectively.

coefficients at temperatures below 100°C (Smithells 1976). Landsat's sensor, with its limited thermal window, simply reads this as being cold without the input of additional information.

Nighttime images are sometimes used in studies, as the heat island's signal shows the sharpest contrast after the peak heating of the day as human-made materials continue to release sensible heat, whereas the surrounding desert environment has cooled (Xian and Crane 2006). Hatchett et al. (2016) further enforces this for the Reno-Sparks high-desert environment, as the stronger growth trend in the UHI signal is seen historically in the minimum temperatures during the summer months.

Imagery used in the study spanned a duration of fourteen years (between 2004 and 2017) of Landsat 7 thermal images. The scene (Row: 211/Path 139) has the Reno-Sparks Metropolitan area in the northern center of the image. As heat island behavior shows the strongest signal in June, July, and August for the Reno-Sparks region (Hatchett et al. 2016), only nocturnal images in, and immediately around, meteorological summertime (the hottest months in the annual temperature cycle in the Northern Hemisphere) were chosen. This set of images was then visually filtered for clouds, with any that contained clouds above the area of interest being rejected, leaving a total of sixty usable images.

All images were georeferenced using major road intersections and prominent building edges as controls (Yuan and Bauer 2007). The raster data were then projected to Universal Transverse Mercator Coordinate system, Zone 11 North, Datum of World Geodetic System of 1984, and then clipped to a smaller spatial area for statistical analysis using the bilinear interpolation approximation method. As the mountains around the valley were not of interest, the clipping footprint was the main body U.S. Census Bureau's 2016 urban boundary that lay within the valley (U. S. Census Bureau 2017). This polygon was additionally convenient, as the majority of it fell within the small band in the center of the scenes that was not impacted by the scan line corrector fault present on Landsat 7 since 2003.

Land surface temperatures were calculated by following the procedure in the Landsat 7 Science Data Users Handbook (Goddard Space Flight Center 2018). The first step was converting the digital number product directly downloaded from Earth Explorer (U. S. Geological Survey-C2018) to Spectral Radiance, done via Equation 1.

Equation 1: Digital Numbers to Spectral Radiance

$$\frac{(Lmax_{\lambda} - Lmin_{\lambda})}{(QCALmax - QCALmin)} * (QCAL - QCALmin) + Lmin_{\lambda}$$

Where:

Lλ = Spectral Radiance at the sensor's aperture (watts/m2*ster*µm)
QCAL = The quantized calibrated pixel value in DN
QCALmin = The minimum quantized calibrated pixel value (corresponding to Lminλ) in DN
QCALmax = The maximum quantized calibrated pixel value (corresponding to Lmaxλ) in DN
Lminλ = The spectral radiance that is scaled to QCALmin (watts/m2*ster*µm)
Lmaxλ = The spectral radiance that is scaled to QCALmax (watts/m2*ster*µm)

The second step was to convert spectral radiance to at-satellite surface temperature in Kelvin using an estimation of Planck's Law of electromagnetic radiation emission via Equation 2 (Yuan and Bauer 2007; Chander and Markham 2003; Goddard Space Flight Center 2018).

Equation 2: Spectral Radiance to at-satellite Temperature

$$T = \frac{K2}{ln\left(\frac{K1}{L_{\lambda}} + 1\right)}$$

Where:

T = Surface Temperature in Kelvin
K1 = Calibration Constant 1 (From scenes' MTL document)
K2 = Calibration Constant 2 (From scenes' MTL document)
Lλ = Spectral Radiance at the sensor's aperture (watts/m2*ster*µm)

To negate the potential of sampling a falsely cold value due to emittance metal roofs, histograms were calculated for all scenes, and values beyond four standard deviations were removed. This value removed the unrealistically cold pixels around the buildings in question, but did not eliminate the lower values seen along waterways or in low-lying fields.

Land cover classifications for this study are defined by the 2001 National Land Cover Database (2001 NLCD) (Homer et al. 2007). Once projected to the same coordinate system as all Landsat images and clipped to the area of interest, they were reclassified into two categories: dry and green (Figure 3). Dry consisted of classes 31 (barren land), 52 (shrub/scrub), and 71 (grassland/herbaceous), with scrublands comprising 72.9% of the undeveloped environment. These three classes represent the standard high-desert environment in which the Reno and Sparks urban cores have grown. Green was a conglomeration of classes 21 (developed open space), 81 (pasture/hay), 82 (cultivated crops), and 95 (emergent herbaceous wetlands). These four classes represent large grass areas around public facilities, city parks, and human-irrigated fields in the region.

The land use dataset covering the entire study area included individual parcels with year built/modified, developed by the Truckee Meadow Regional Planning Agency (Truckee Meadows Regional Planning Agency 2017) and was used to determine areas that had been developed during the study period (Figure 4). This map shows properties that were constructed between 2004 and 2017 and used to determine green built and dry built. The area developed totaled approximately 23.2 km^2 or 5,733 acres (Figure 5). Parcels that had been built in 2001 through 2004 were masked out of the 2001 NLCD, as Landsat has few nighttime flyovers of the Reno-Sparks region during that time frame. Changes in land cover class between 2001 and 2004 were accounted for by referencing this dataset.

The processed Landsat images were grouped by year, and at-satellite temperature was averaged on a pixel-by-pixel basis, as the parcel data was only described to the year level. This also helped to account for meteorological variations for each year. This yearly average temperature value was converted into a spatial data table with columns of whether the pixel was developed or unaltered and whether it was originally dry land cover or green. This created four classes with associated temperatures: dry built, green built, dry unbuilt, and green unbuilt for each year.

All years were combined into a single spatial data table (Figure 6), and then a stratified random sample with a size of 300 per class, per year, was conducted on the records in this dataset (Figure 7). This resulted in a total of 1,200 per year and a grand total of 15,600. As hundreds of thousands of records existed within the main spatial data table, it was deemed that 300 should be able to capture the variation of each of the four classes at a high confidence level without increasing the chance of a convergence of proba-

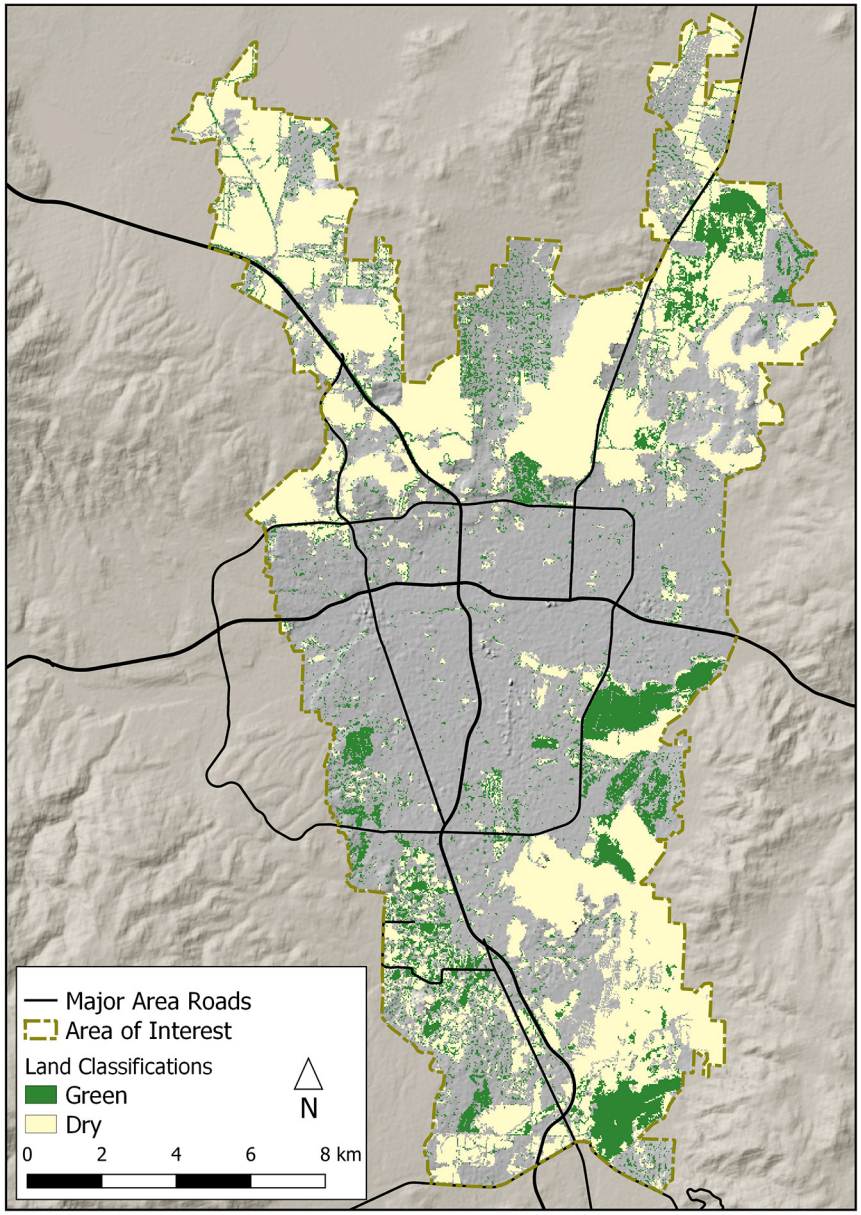

Figure 3.—Dry and Green Classified regions in the study area AOI.

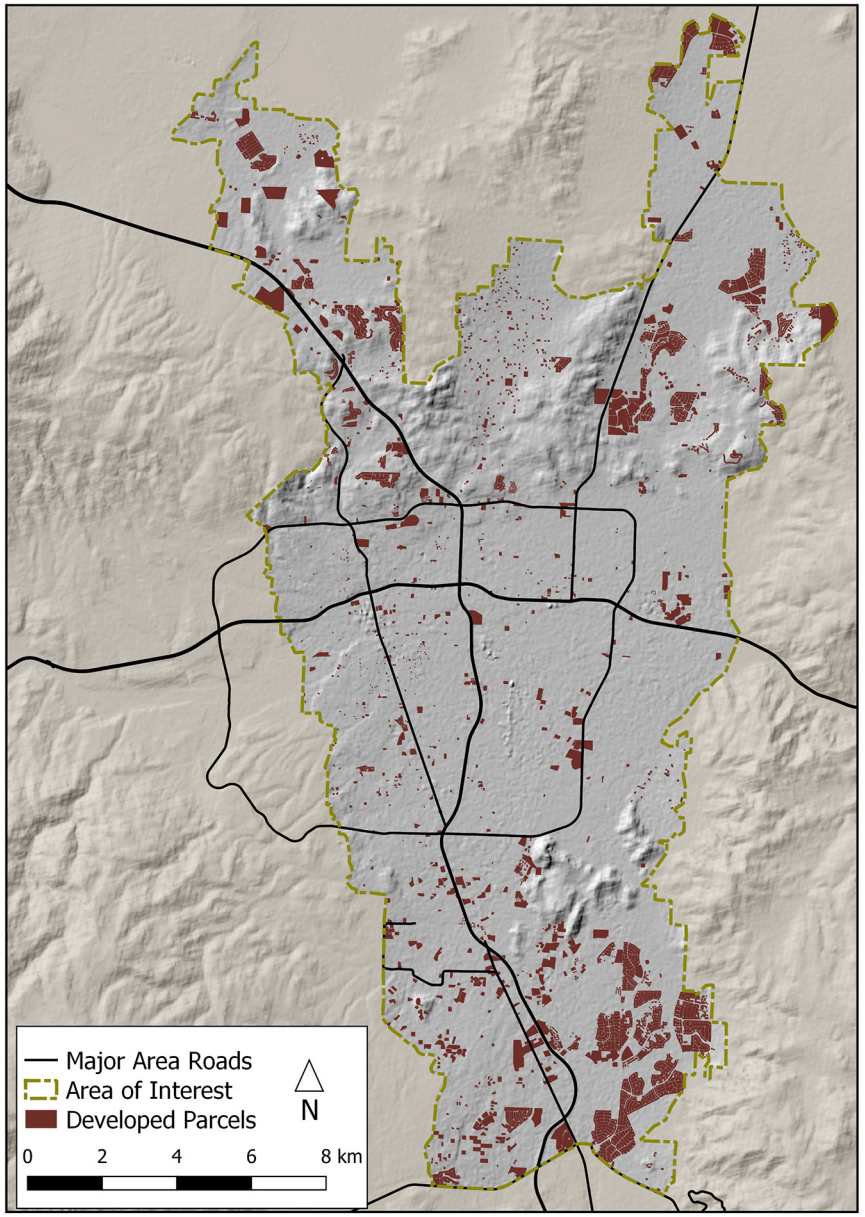

Figure 4.—Parcels that had undergone development between the years of 2004 and 2017 in the AOI.

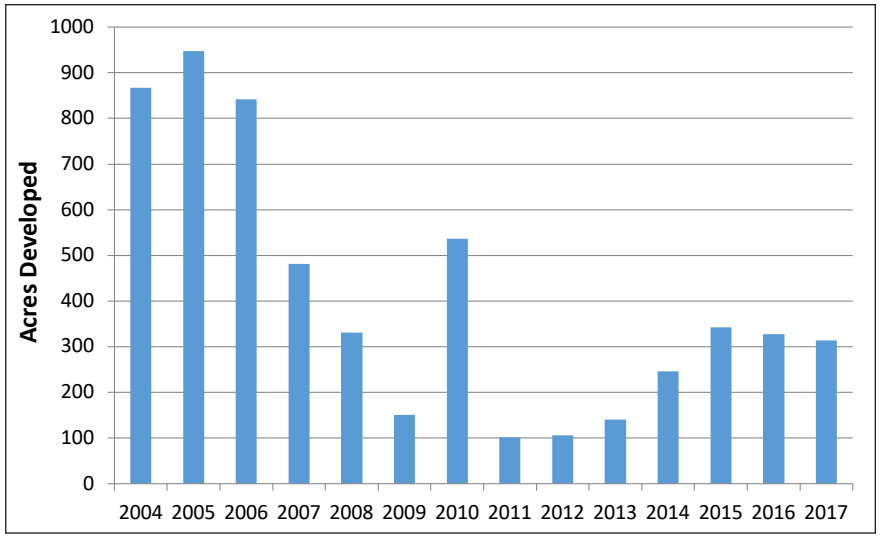

Figure 5.—Bar chart of approximate acreage built per year.

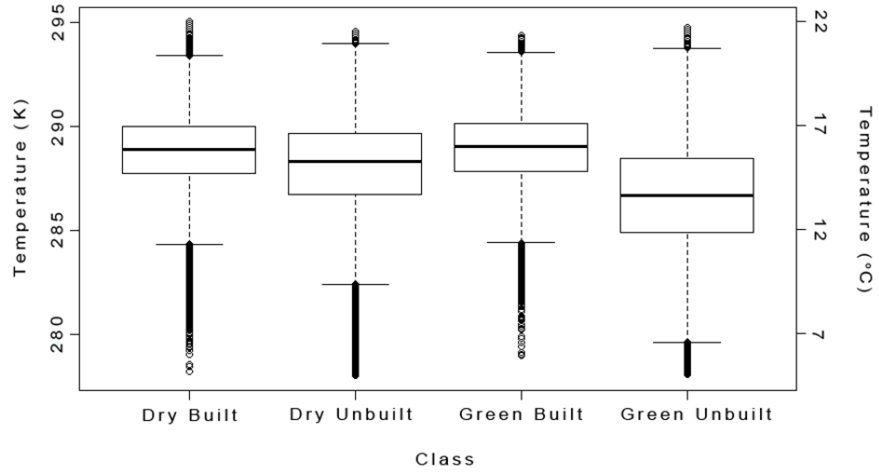

Figure 6.—Boxplot of all data for all years, categorized by Land Cover Class.

bilities (Cochran 1977; Israel 1992; Fischer 2010). A Cross-Validation was completed to assess the effectiveness of the model. A total of ten random iterations were completed with the same sample parameters on the population of the spatial points data frame.

A set of general linear models were fit to the sampled data. Models included a null model with "Temperature only," another with the predictor variable of "Land Cover Class," a third with the temporal changes between each

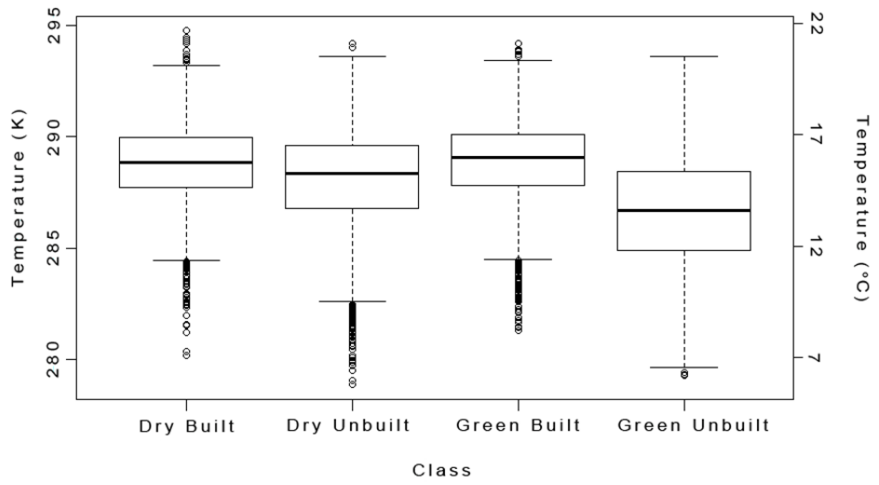

Figure 7.—Boxplot of all samples for all years, categorized by Land Cover Class.

"Year," and fourth and finally a model with an interaction between the terms "Land Cover Class" and "Year." Akaike's Information Criterion (AIC) was chosen as the determinant of the relatively best fit model (Akaike 1974). A pair-wise comparison was completed to evaluate results of the Generalized Linear Model. This contrast test is known as Tukey's Honestly Significant Difference Test, and summarizes statistical relationships (Tukey 1949). An analysis of variance F-Test that was also conducted on the main effects showed significant differences between the land cover classes (F-Statistic of 1,390.8) ($P < 0.001$).

Results

The model with "Year" interaction with "Land Cover Class" had the lowest AIC estimate (Table 1). This proves "Land Cover Class" explains most of the temperature variance, but the model can be reasonably improved upon by adding the year to year variability in temperature. The generalized linear model showed a surface temperature for the area of interest of 288.68 K or 15.53°C (Table 2) with an R-squared of 0.40. Cross-validation had a mean correlation coefficient of 0.623 (standard deviation of 0.008) compared to the model's 0.624.

Table 1. AIC Table

	Intercept	degrees freedom	AIC	delta	weight
Land Cover Class * Year	288.7	53	62,437.0	0.0	1
Year	288	14	65,610.6	3,173.6	0
Land Cover Class	288.8	5	66,682.1	4,375.1	0
Null (Temperature)	288.1	2	69,392.4	6,955.4	0

Table 2. Generalized Linear Model output

Note: Estimate is in Kelvin. Signif Codes are as follows: 0 '*' , 0.001 '**', 0.5 '*', 0.1 '.'*

Coefficients	Estimate	Std. Error	t value	Pr(>|t|)	signif. code
Intercept	288.675	0.102	2834.658	< 2e -16	***
Dry Unbuilt	-0.635	0.144	-4.412	1.03e - 05	***
Green Built	0.087	0.144	0.604	0.5458	
Green Unbuilt	-2.237	0.144	-15.53	< 2e -16	***
year 2005	0.262	0.144	1.816	0.0694	.
year 2006	1.722	0.144	11.956	< 2e -16	***
year 2007	-0.379	0.144	-2.632	0.0085	**
year 2008	-0.670	0.144	-4.832	1.37e - 06	***
year 2009	0.893	0.144	6.201	5.77e -10	***
year 2010	-2.037	0.144	-14.146	< 2e -16	***
year 2011	0.060	0.144	0.419	0.6751	
year 2012	1.190	0.144	8.263	< 2e -16	***
year 2013	-0.902	0.144	-6.263	3.88e -10	***
year 2014	-0.564	0.144	-3.918	8.98e - 05	***
year 2016	0.200	0.144	1.390	0.1645	
year 2017	1.612	0.144	11.192	< 2e -16	***
Dry Unbuilt : Year 2005	-0.326	0.204	-1.602	0.1092	
Green Built : Year 2005	0.060	0.204	0.296	0.7675	
Green Unbuilt : Year 2005	-0.105	0.204	-0.516	0.6062	
Dry Unbuilt : Year 2006	0.107	0.204	0.525	0.5997	
Green Built : Year 2006	-0.295	0.204	-1.449	0.1474	
Green Unbuilt : Year 2006	-0.051	0.204	-0.253	0.8002	
Dry Unbuilt : Year 2007	-0.086	0.204	-0.420	0.6746	
Green Built : Year 2007	-0.076	0.204	-0.374	0.7085	
Green Unbuilt : Year 2007	0.081	0.204	0.399	0.6902	
Dry Unbuilt : Year 2008	-0.198	0.204	-0.974	0.3300	
Green Built : Year 2008	-0.460	0.204	-2.260	0.0238	*
Green Unbuilt : Year 2008	-0.029	0.204	-0.142	0.8870	
Dry Unbuilt : Year 2009	-0.235	0.204	-1.152	0.2492	
Green Built : Year 2009	-0.105	0.204	-0.517	0.6050	
Green Unbuilt : Year 2009	0.301	0.204	1.475	0.1401	
Dry Unbuilt : Year 2010	-0.225	0.204	-1.104	0.2695	
Green Built : Year 2010	-0.021	0.204	-0.101	0.9198	
Green Unbuilt : Year 2010	0.195	0.204	0.960	0.3372	
Dry Unbuilt : Year 2011	0.398	0.204	1.953	0.0509	.
Green Built : Year 2011	0.065	0.204	0.321	0.7483	
Green Unbuilt : Year 2011	-0.102	0.204	-0.505	0.6132	
Dry Unbuilt : Year 2012	-0.110	0.204	-0.539	0.5898	
Green Built : Year 2012	0.242	0.204	1.193	0.2329	
Green Unbuilt : Year 2012	0.226	0.204	1.109	0.2673	
Dry Unbuilt : Year 2013	-0.171	0.204	-0.842	0.3998	
Green Built : Year 2013	0.144	0.204	0.710	0.4778	
Green Unbuilt : Year 2013	0.380	0.204	1.868	0.0617	.
Dry Unbuilt : Year 2014	-0.451	0.204	-2.218	0.0265	*
Green Built : Year 2014	0.130	0.204	0.642	0.5209	
Green Unbuilt : Year 2014	0.281	0.204	1.381	0.1674	
Dry Unbuilt : Year 2016	0.381	0.204	1.869	0.0616	.
Green Built : Year 2016	0.156	0.204	0.768	0.4426	
Green Unbuilt : Year 2016	0.155	0.204	0.761	0.4467	
Dry Unbuilt : Year 2017	0.220	0.204	1.081	0.2799	
Green Built : Year 2017	0.031	0.204	0.149	0.8814	
Green Unbuilt : Year 2017	0.321	0.204	1.576	0.1150	

Areas that originated as the green unbuilt class constructed during the study period showed no significant change between the expected pre-developed temperature (a difference of 0.087°C). The surrounding dry unbuilt class within the area of interest had a cooler temperature than the model's expected value, with a change of -0.64°C ($P < 0.001$). The green built landscape was

approximately 2.24°C cooler than the intercept of the null model ($P < 0.001$). The GLM output shows a significant difference between many of the years, further compounding that one or two years of temperature data may not fully describe an area's, region's, or city's thermal regimes. Tukey's Test also identified a significant difference between all land cover classes except for green built versus dry built (Table 3).

Table 3. Tukey's Honest Significant Difference

Note: Estimate is in Kelvin/degrees Celsius. Signif Codes are as follows: 0 '*' , 0.001 '**', 0.5 '*', 0.1 '.'*

Class Contrast	Estimate	Std. Error	z value	Pr (>|z|)	Signif. code
Dry Unbuilt - Dry Built	-0.635	0.14402	-4.412	< 1e - 04	***
Green Built - Dry Built	0.087	0.14402	0.604	0.931	
Green Unbuilt - Dry Built	-2.237	0.14402	-15.530	< 1e - 04	***
Green Built - Dry UnBuilt	0.722	0.14402	5.016	< 1e - 04	***
Green Unbuilt - Dry UnBuilt	-1.601	0.14402	-11.118	< 1e - 04	***
Green Unbuilt - Green Built	-2.324	0.14402	-16.134	< 1e - 04	***

Discussion

The nighttime surface thermal environment is altered by development, and to a much greater degree if the land developed was originally green built. Of an original 91.0 km^2 of dry unbuilt within the area of interest, a total of approximately 18.2 km^2 was developed between 2004 and 2017. Of an original 29.5 km^2 of green unbuilt within the study zone, approximately 4.6 km^2 was developed. I use approximate numbers because a parcel may have been carved out of a larger section and declared by the county as developed in a certain year, but the construction of the entire footprint of a parcel may not have occurred within that exact year. Some parcels were also slated for development as lower-density suburban housing. Areas featuring mixed pixels as yards and other personal greenspace have an increasing trend in the American West (Yabiku et al. 2008). Many parcels did not undergo a 100 percent change from one landcover class to a new one. Most suburban homes, for example, are designed with a front and/or back yard, and thus are not a true 100 percent change of class from green unbuilt or dry unbuilt. As a result, a broad area's true temperature change is not the same as would be seen with a much smaller, more homogeneous cover. However, value changes of one and two degrees Celsius when developed are not unexpected for the Southwestern United States (Cayan and Douglas 1984).

While the National Land Cover Database is freely available and a versatile product, it does have some inaccuracies, as can be expected with any remotely sensed product (Wickham et al. 2010). Additional inaccuracy also may have been introduced by the area's wetlands' water content changing over time (Pavri and Aber 2004). Both of these previous factors would have impacted how well the original NLCD classes matched what was truly in the valley, and therefore how well this research's four classes (dry unbuilt, dry built, green unbuilt, green built) would have performed in representing the actual land cover.

Development during the study period does not seem to override the influences of the local climate or topography to any observable degree, as direct comparisons of the total area of interest's surface thermal signal over the study period did not return any significant trends. This means that while undeveloped regions in the area of interest showed a significant increase in surface temperature after being developed, the climatology for Reno-Sparks as a whole does not seem to have been impacted for the duration of 2004 through 2017.

Some years were warmer or colder/wetter or drier than others. Landsat passes over only once every sixteen days, severely limiting the sample size of each year and the ability to correct for abnormal years and conditions. This is especially important in a steppe environment, where small differences in available moisture can be a large driver of vegetative health and density (Moore et al. 2015). The yearly variations in temperature and precipitation trends made a quantifiable, citywide change in the surface urban heat island's signal difficult to detect, due to the city's relatively small size and location nestled between multiple mountain ranges.

A positive shift in temperature of 0.6°C to the native landscape steppe cover, 8.2 percent of the entire area of interest's footprint, was clearly seen. The paving over of green space was the more noteworthy driver of change, with a 2.2°C temperature increase. However, only 4.6 km^2 of green space was built during the past fourteen years. This is less than 1.7 percent of the total area of interest, or a total of 15.6 percent of green space present in the area of interest. Reno-Sparks' growth was encumbered during multiple years of the research's imagery period, due to the National Recession in 2008 (Truckee Meadows Regional Planning Agency 2017). There was no significant difference between developed land originating as either green unbuilt or dry unbuilt.

While expansion into green space in Reno-Sparks was negligible for the years between 2004 and 2017, subdivisions are currently being constructed into the area's wetlands. Current plans also show numerous additional units slated for the next few years expanding into the valley's southeast wetlands and agricultural lands, as well as into alluvial catch basins along the mountain fronts (Truckee Meadows Regional Planning Agency 2017). If development follows current plans, it can be expected that the Reno-Sparks UHI will continue to expand and possibly show even stronger signals through the next decades, as development covers a higher fraction of greenspace than it did since 2004.

Conclusions

In this research, a series of sixty Landsat 7 thermal images covering fourteen years of development in the Reno-Sparks metropolitan area were analyzed. Spaces that had been developed from natural desert grasses and sage (dry unbuilt) showed a surface temperature increase of 0.6°C. Portions that had been developed from green unbuilt, be it natural or human-made green space, showed a 2.2°C increase in surface temperature. Since these areas of change account for 18.2 and 4.6 km^2 respectively, Reno-Sparks' UHI signal has measurably increased since the turn of the millennium.

Not all development is equal, and future work could be done to account for varying degrees of impervious surfaces throughout Reno-Sparks. Suburban versus more intensely developed areas such as industrial or highly urbanized zones could be individually categorized, and planners/policy makers will be able to better allot for the potential change in surface heat retention to result in less contribution to the UHI.

Due to income disparities, the development of green spaces in urban landscapes is inequitable. This disproportion is seen in the percentage of green space within a given neighborhood, with a significant positive gradient in green space following economic classes in southwestern U.S. metropolitan areas (Jenerette et al. 2013). This owes to the wealthier classes generally living in lower density areas, thus dwelling upon larger lots and being more likely to have access to the resources to landscape/manage them as well (Clarke et al. 2013). Socioeconomic data for Reno-Sparks could determine to what extent income divergence exposes its citizens to UHI impacts, and whether or not future planned regions of the valley perpetuate this.

The UHI phenomena will continue to be a feature of the global landscape, exacerbated by the world's growing population, by the trend of urbanization of this population, and by meteorological extremes/climate change (IPCC 2014).In order to mitigate this human-created issue, we must first understand it and its unique fingerprint within every city. This type of data was a premium before the 1970s and therefore was unavailable to many. With the advancements of remote sensing, it is now available at no cost. Landsat thermal data is available for the majority of the Earth's surface, and looks to be so in the future with the recent Landsat 8 and upcoming Landsat 9 (to be launched in the end of 2020); it is hoped that this research can provide a template for future studies. With remote sensing and ever-advancing technologies, UHIs can be studied in a greater temporal and spatial resolution in many small and growing cities throughout the world.

References

Akaike, H. 1974. A new look at the statistical model identification. *IEEE Transactions on Automatic Control* 19 (6):716–723.

Akbari, H., M. Pomerantz, and H. Taha. 2001. Cool surfaces and shade trees to reduce energy use and improve air quality in urban areas. *Solar Energy* 70 (3):295–310.

Aniello, C., K. Morgan, A. Busbey, and L. Newland. 1994. Mapping micro-urban heat islands using Landsat TM and a GIS. *Computers & Geosciences* 21 (8):965–969.

Arndt, D. S., and K. T. Redmond. 2004. Toward an automated tool for detecting relationship changes within a series of observations. American Meteorological Society Annual Meeting, Applied Climatology Conference, January 11–15, 2004, Seattle, Washington.

Azevedo, J. A., L. Chapman, and C. I. Muller. 2016. Urban heat and residential electricity consumption: A preliminary study. *Applied Geography* 70:59–67.

Bokaie, M., M. K. Zarkesh, P. D. Arasteh, and A. Hosseini. 2016. Assessment of urban heat island based on the relationship between land surface temperature and land use/land cover in Tehran. *Sustainable Cities and Society* 23:94–104.

Cayan, D. R., and A. V. Douglas. 1984. Urban influences on surface temperatures in the Southwestern United States during recent decades. *Journal of Climate and Applied Meteorology* 23:1520–1530.

Chander, G., and B. Markham. 2003. Revised Landsat-5 TM radiometric calibration procedures and postcalibration dynamic ranges. *IEEE Transactions on Geoscience and Remote Sensing* 41 (11):2674–2677.

Clarke, L. W., G. D. Jenerette, and A. Davila. 2013. The luxury of vegetation and the legacy of tree biodiversity in Los Angeles, CA. *Landscape and Urban Planning* 116:48–59.

Cochran, W. G. 1977. *Sampling Techniques (3rd Edition)*. Hoboken, NJ: John Wiley & Sons, Inc.
Estoque, R. C., Y. Murayama, and S. W. Myint. 2017. Effects of landscape composition and pattern on land surface temperature: An urban heat island study in the Megacities of Southeast Asia. *Science of the Total Environment* 577:349–359.
Fischer, H. 2010. A *History of the Central Limit Theorem*. New York, NY: Springer.
Forstall, R. L. 1996. Population of States and Counties of the United States: 1790–1990. U.S. Department of Commerce, National Technical Information Service, Springfield, VA.
Gillner, S., J. Vogt, A. Tharang, S. Dettmann, and A. Roloff. 2015. Role of street trees in mitigating effects of heat and drought at highly sealed urban sites. *Landscape and Urban Planning* 143:33–42.
Goddard Space Flight Center, National Aeronautics and Space Administration. 2018. *Landsat 7 Science Data Users Handbook*; Greenbelt, Maryland. https://landsat.gsfc.nasa.gov/wp-content/uploads/2016/08/Landsat7_Handbook.pdf
Hatchett, B. J., D. Koračin, D., J. F. Mejía,and D. P. Boyle. 2016. Assimilating urban heat island effects into climate projections. *Journal of Arid Environments* 128:59–64.
Homer, C., J. Dewitz, J. Fry, M. Coan, N. Hossain, C. Larson, N. Herold, A. McKerrow, J. N. VanDriel, and J. Wickham. 2007. Completion of the 2001 National Land Cover Database for the Conterminous United States. *Photogrammetric Engineering and Remote Sensing* 73 (4):337–341.
Houghton, J. G., C. M. Sakamoto, and R. O. Gifford. 1975. *Nevada's Weather and Climate.* Special Publication 2. Nevada Bureau of Mines and Geology, Mackay School of Mines, University of Nevada, Reno.
Imhoff, M. L., P. Zhang, R. E. Wolfe, and L. Bounoua. 2010. Remote sensing of the urban heat island effect across biomes in the continental USA. *Remote Sensing of Environment* 114 (3):504–513.
IPCC. 2014: Climate Change 2014: Synthesis Report. Contribution of Working Groups I, II and III to the Fifth Assessment Report of the Intergovernmental Panel on Climate Change [Core Writing Team, R. K. Pachauri and L. A. Meyer (eds.)]. IPCC, Geneva, Switzerland.
Israel, G. D. 1992. Determining Sample Size. University of Florida. Florida Cooperative Extension Office, Fact Sheet PEOD-6
Jenerette, G. D., G. Miller, A. Buyantuev, D. E. Pataki, T. W. Gillspie, and S. Pincetl. 2013. Urban vegetation and income segregation in drylands: a synthesis of seven metropolitan regions in the southwestern United States. *Environmental Research Letters* 8.
Jones, B., B. C. O'Neill, L. McDaniel, S. McGinnis, L. O. Mearns, and C. Tebaldi. 2015. Future population exposure to US heat extremes. *Nature Climate Change* 5:652–655.
Mason, T., F. Brivio, P. Stephens, M. Apollonio, and S. Grignolio. 2017. The behavioral trade-off between thermoregulation and foraging in a heat-sensitive species. *Behavioral Ecology* 28 (3):909–918.
Mirzaei, P., and F. Haghighat. 2010. Approaches to study Urban Heat Island – Abilities and limitations. *Building and Environment* 45:2192–2201.
Moore, L. M., W. K. Lauenroth, D. M. Bell, and D. R. Schlaepfer. 2015. Soil Water and Temperature Explain Canopy Phenology and Onset of Spring in a Semiarid Steppe. *Great Plains Research, University of Nebraska Press* 25 (2):121–138.
Morton, C. 2018. Personal interview conducted at Desert Research Institute, Reno, NV; November 29.
Northern Nevada Regional Growth Study 2015–2019, Volume I: A Forecast of Northern Nevada's Employment, Population, Households & Associated Tax Revenues. Economic Planning Indicators Committee, Economic Development Authority of Western Nevada. 2015. http://edawn.org/wp-content/uploads/2015/09/2015-8-31-Vol-1-No-NV-Regional-Growth-Study-Final_Compressed.pdf
Oke, T. R. 1973. City size and the urban heat island. *Atmospheric Environment* 7 (8):769–779.
Pavri, F., and J. S. Aber. 2004.Characterizing Wetland Landscapes: A Spatiotemporal Analysis of Remotely Sensed Data at Cheyenne Bottoms, Kansas. *Physical Geography* 25 (1):86–104.
Rahman, R. A., A. Moser, T. Rotzer, and S. Pauleit. 2017. Within canopy temperature differences and cooling ability of *Tiliacordata* trees grown in urban conditions. *Building and Environment* 114:118–128.
Ramamurthy, P., and M. Sangobanwo. 2016. Inter-annual variability in urban heat island intensity over 10 major cities in the United States. *Sustainable Cities and Society* 26:65–75.
Robine, J. M., S. L. Cheung, S. Le Roy, H. Van Oyen, C. Griffiths, J. P. Michel, and F. R. Herrmann. 2007. Death toll exceeded 70,000 in Europe during the summer of 2003. *La Revue Du Praticien* 54 (12):1289–1297.
Small, C., and C. Zappa. 2017. Mapping the diurnal thermal response of the urban heat island with Landsat TIRS. *IEEE Joint Urban Remote Sensing Event (JURSE), 2017*:1–4.

Smithells, C. J. 1976. *Metals Reference Book, 5th edition*. London: Butterworth & Co. Industrial Estate Chichester.
Truckee Meadows Regional Planning Agency. 2017. Land Use Fabric Dataset.
Tukey, J. 1949. Comparing Individual Means in the Analysis of Variance. *Biometrics* 5 (2):99–114.
United Nations. 2014. *World Urbanization Prospects 2014 Revision*. UN DESA's Population Division, New York, NY.
U.S. Census Bureau, U.S. Department of Commerce. 2017. 2016 Cartographic Boundary File, 2010 Urban Areas for United States. 4600 Silver Hill Road, Washington, D.C.
U.S. Geological Survey. 2006. Shuttle Radar Topography Mission. 1 Arc Second Scene, Global Land Cover Facility, University of Maryland, College Park, 2000.
U.S. Geological Survey-A, U.S. Department of the Interior. 2018. *What are the band designations for the Landsat satellites?* Web. Updated: April 25, 2018 https://landsat.usgs.gov/what-are-band-designations-landsat-satellites
U.S. Geological Survey-B, U.S. Department of the Interior. 2018. Landsat 7 Data Users Handbook – Section 5. https://landsat.usgs.gov/landsat-7-data-users-handbook-section-5
U.S. Geological Survey-C, U.S. Department of the Interior. 2018. Earth Explorer-Home. https://earthexplorer.usgs.gov/
Wang, Y., and H. Akbari. 2016. Analysis of urban heat island phenomena and mitigation solutions evaluation for Montreal. *Sustainable Cities and Society* 26:438–446.
Washoe County Consensus Forecast 2016–2036. Truckee Meadows Regional Planning. 2016. http://www.tmrpa.org/files/reports/16-09-28%20WC%20Consensus%20Forecast%202016%20Final%20with%20Appendices.pdf
Wang, Q., and D. A. Quattrochi. 2007. *Urban Remote Sensing*. Boca Raton, FL: CRC Press, Taylor and Francis Group.
Wickham, J. D., S. V. Stehman, J. A. Fry, J. H. Smith, and C. G. Homer. 2010. Thematic accuracy of the NLCD 2001 land cover for the conterminous United States. *Remote Sensing of Environment* 114 (6):1286–1296.
Xian, G., and M. Crane. 2006. An analysis of urban thermal characteristics and associated land cover in Tampa Bay and Las Vegas using Landsat satellite data. *Remote Sensing of Environment* 104 (2):147–156.
Yabiku, S. T., D. G. Casagrande, and E. Farley-Metzger. 2008. Preferences for Landscape Choice in a Southwestern Desert City. *Environment and Behavior* 40 (3):382–400.
Yuan, F., and M. E. Bauer. 2007. Comparison of impervious surface area and normalized difference vegetation index as indicators of surface urban heat island effects in Landsat imagery. *Remote Sensing of Environment* 106:375–386.